ISSN PRINT 2319 1775 Online 2320 7876

Research paper © 2012 IJFANS. All Rights Reserved, UGC CARE Listed (Group -I) Journal Volume 11, Iss 8, Dec 2022

Effect of *Pedalium murex* extract assist biosynthesized spinel $CoFe_2O_4$ magnetic nanoparticles for enhanced photocatalytic and antibacterial applications

K. Thanrasu [1,*], A. Dinesh [1], K. Kanmani Raja [1,*]

[1] Department of Chemistry, Government Arts College for Men (Autonomous), Affiliated to the University of Madras, Nandanam, Chennai – 600035, Tamil Nadu, India

***Corresponding Author Email addresses:** kthanrasut@gmail.com (K. Thanrasu); kkanmaniraja@gmail.com (K. Kanmani Raja)

Abstract

In this study, cobalt ferrite ($CoFe_2O_4$) magnetic nanoparticles were biosynthesized using *Pedalium murex* leaf extract by microwave combustion method ($CoFe_2O_4$-MCM) and convention combustion method ($CoFe_2O_4$-CCM) for comparative study purpose. Physicochemical properties of the $CoFe_2O_4$ nanoparticles were determined by high resolution transmission electron microscopy (HR-TEM), High resolution scanning electron microscopy (HR-SEM), Powder X-ray diffraction (XRD), vibrating sample magnetometer (VSM), and energy dispersive X-ray (EDX) mapping analysis. The XRD diffractograms confirmed the cubic $CoFe_2O_4$ nanoparticles. FTIR data showed the presence of the metal-oxygen vibration. HR- SEM images demonstrated the sphere shaped particles with nano range, and EDX further approved the existence of the element. The grown samples were tested for antibacterial disinfection, and $CoFe_2O_4$-MCM nanoparticles sample showed a higher zone of inhibition against gram-positive *S. aureus (Staphylococcus aureus*), *B. subtilis* (*Bacillus subtilis*) *and* gram-negative *E. coli (Escherichia coli)* and *K. pneumonia (Klebsiella pneumoniae)* bacteria strains. Furthermore, the results showed that the photocatalytic and antibacterial, performance of $CoFe_2O_4$-MCM nanoparticles could be enhanced by particle size and temperature effect. It appears that these nanostructures can be considered as suitable candidates for drug delivery and other biomedical applications, because of their toxicity effects.

Keywords: *Pedalium murex* leaf extract; $CoFe_2O_4$ nanoparticles; microwave combustion; photocatalytic performance; antibacterial study.

1. Introduction

Nanoparticles of ferrites with large coercivity and saturation magnetization are generally used in making the recording devices, permanent magnets, electric motors, automotive power etc. The coercivity and saturation magnetization properties are improved by varying chemical composition and micro-structural characteristics. Ferrite nanoparticles are also applied in chemical reactions due to their catalytic, photo catalytic, and photo electrochemical properties [1-2].

In recent decades, spinel ferrite magnetic nanoparticles (MNPs) with the chemical formula of MFe_2O_4 (M: divalent metal ions, e.g. Mn, Cu, Zn, Cu, etc.) have attracted the much attention of researchers in various applications such as biomedical fields including drug delivery, sensor materials, catalytic and energy storage devices, etc [3-5]. The excellent

ISSN PRINT 2319 1775 Online 2320 7876

Research paper **© 2012 IJFANS. All Rights Reserved, UGC CARE Listed (Group -I) Journal Volume 11, Iss 8, Dec 2022**

properties of spinel ferrites are well utilized in modern technological applications. Ferrites often have a spinel structure with the formula AB_2O_4, where A and B are various metal cations, with iron being the most common (Fe). Spinel ferrites are of particular importance in photocatalyst, electronic devices, and storage materials and they also can be employed as magnetic resonance imaging (MRI) contrast agents [6-10]. Spinel ferrites typically adopt FCC oxides (O^{2-}) with A cations reside in one-eighth of the tetrahedral holes and B cations reside in half of the octahedral holes, i.e. instead of the normal spinel structure, ferrite crystals have the inverse spinel structure: B cations occupy (1/8)th of the tetrahedral holes, A cations occupy (1/4)th of the octahedral sites, and B cations occupy the remaining (1/4)th octahedral sites. Spinel ferrites with a mixed structure can also be possible with the formula $[M_{1-\delta}^{2+}Fe_{\delta}^{3+}][M_{\delta}^{2+}Fe_{2-\delta}^{3+}]O_4$, here δ represents the degree of inversion [11-13]. Also, ferrites are hard, brittle, iron-containing, and generally grey or black and are polycrystalline materials.

Spinel ferrites have vast domains application in the present technological world. The main applications are precursors for Ferro-fluids, radio, magnetic guided drug-delivery agents, telecommunication, biomedicine, magnetic storage, gas sensor, television, microwave, military devices, microwave absorbers, satellite communication, humidity sensors and magnetic storage [14-17]. Among them, the $CoFe_2O_4$ is an important material with good chemical stability, moderate magnetization, high sensitivity, band gap of ~2.0 eV, and high electrical resistivity, and it is widely used in the transformer core, gas sensor, anode materials, photocatalysis and microwave absorber [18]. Spinel $CoFe_2O_4$ nanoparticles exhibit spinel cubic structure. Spinel $CoFe_2O_4$ is a kind of lenient magnetic material among different ferrites with little saturation magnetization (Ms) and coercivity (Hc). They are used for sensing gases and temperature, and for catalytic applications. Spinel $CoFe_2O_4$ nanoparticles have been shown to be superparamagnetic or ferrimagnetic depending on its size. Spinel $CoFe_2O_4$ nanoparticles with a size smaller than 15 nm behave as a superparamagnetic material and those above 15 nm behave as ferrimagnetic materials. The oxygen atoms in ferrites surround the metal ions, resulting in a superexchange interaction between the A- and B- sublattices, which disturbs ferrites' magnetic properties [19]. These interesting properties motivated us to choose spinel $CoFe_2O_4$ magnetic nanoparticles for the present study.

Generally, Cobalt ferrites can be easily separated after the reaction, reusability also magnetic and catalytic recyclability makes more attraction among young researchers. Furthermore, unique mixture of large coercivity with moderate magnetized properties support it as aneffective hard magnetic material. These can generate $CoFe_2O_4$ nanoparticles seemly for magnetic recording applications such as audio and video tape and high-density numerical recording disks etc. [20-23].

Precursors of metal nitrates and the fuel *Pedalium Murex* plant extract in a suitable stoichiometric ratio encourage the exothermic and self-sustaining reaction by the combustion process as per the propellant chemistry principle. The suitable plant extract fuels are usually *Aloe vera*, *Sesamum indicum*, *Hibiscus rosa-sinensis*, *Abelmoschus esculentus*, *Pedalium Murex,* and *Opuntia dillenii*. To the best of our knowledge, only a limited number of articles discussed the influence of synthesis method on the morphology, crystal structure, and magnetic properties of spinel $CoFe_2O_4$ nanoparticles. Spinel $CoFe_2O_4$ MNPs are ceramic nanoscale materials [24], which can be used photocatalytic and biological applications. In this study, cobalt ferrite MNPs were eco-friendly synthesized using aqueous extract of *Pedalium murex*. The physicochemical properties of these $CoFe_2O_4$ MNPs were determined by high resolution transmission electron microscopy (HR-TEM), high resolution scanning electron microscopy (HR-SEM), powder X-ray diffraction (XRD), vibrating sample magnetometer

ISSN PRINT 2319 1775 Online 2320 7876

Research paper **© 2012 IJFANS. All Rights Reserved, UGC CARE Listed (Group -I) Journal Volume 11, Iss 8, Dec 2022**

(VSM), and energy dispersive X-ray (EDX) mapping analysis. In the present work, for the first time, we investigated the structural, morphological, and photocatalytic properties of spinel $CoFe_2O_4$ nanoparticles and the obtained results are reported in detail herein.

2. Experimental part

2.1 Chemicals

All the chemicals used in this study were of analytical grade obtained from Merck, India and were used as received without further purification. Ferric nitrate ($Fe(NO_3)_3 \cdot 9H_2O$, 98%), cobalt nitrates ($Co(NO_3)_2 \cdot 6H_2O$, 98%) and *Pedalium Murex* plant extract as the raw materials were used for these methods.

2.2 Synthesis of *Pedalium Murex* plant extract

The *Pedalium Murex* leaves were collected from the local agricultural fields, Athanur, Peravurani, Thanjavur District, Tamil Nadu State, India. *Pedalium Murex* extract was prepared from a 5 g portion of thoroughly washed *Pedalium Murex* leaves were finely cut and the gel obtained was dissolved in 10 ml of de-ionized water and stirred for 30 min to obtain a clear solution. The resulting product was used as *Pedalium Murex* plant extract.

2.3 Synthesis of $CoFe_2O_4$ by microwave combustion method

In the preparation of $CoFe_2O_4$ samples, ferric nitrate (10 mmol) and cobalt nitrate (5 mmol) were first dissolved in the *Pedalium Murex* plant extract under vigorous stirring at room temperature for 1 h until a clear transparent solution was obtained. In this preparation process, *Pedalium Murex* plant extract has a double function of both reducing and gelling agent for the synthesis of mixed metal oxides. Metal nitrate salts and the *Pedalium Murex* plant extract were chosen by considering the total reducing and oxidizing agent valences of the raw materials and were quantified in equivalence of NOx reduction (N_2O to N_2, CO_2 and H_2O) at a low temperature. The precursor mixture of metal nitrates in *Pedalium Murex* plant extract was placed in a domestic microwave oven and exposed to the microwave energy in a 2.45 GHz multimode cavity at 950 W for 10 min. Initially, the precursor mixture boiled and underwent evaporation followed by the decomposition with the evolution of gases. When the solution reached the point of spontaneous combustion, it vaporized and instantly became a solid. After completion of the reaction, the obtained solid powder was then washed with ethanol and dried at 70 ℃ for 1h. The obtained powders were labelled as $CoFe_2O_4$-MCM, which was obtained by MCM approach (**Scheme 1**).

ISSN PRINT 2319 1775 Online 2320 7876

Research paper **© 2012 IJFANS. All Rights Reserved, UGC CARE Listed (Group -I) Journal Volume 11, Iss 8, Dec 2022**

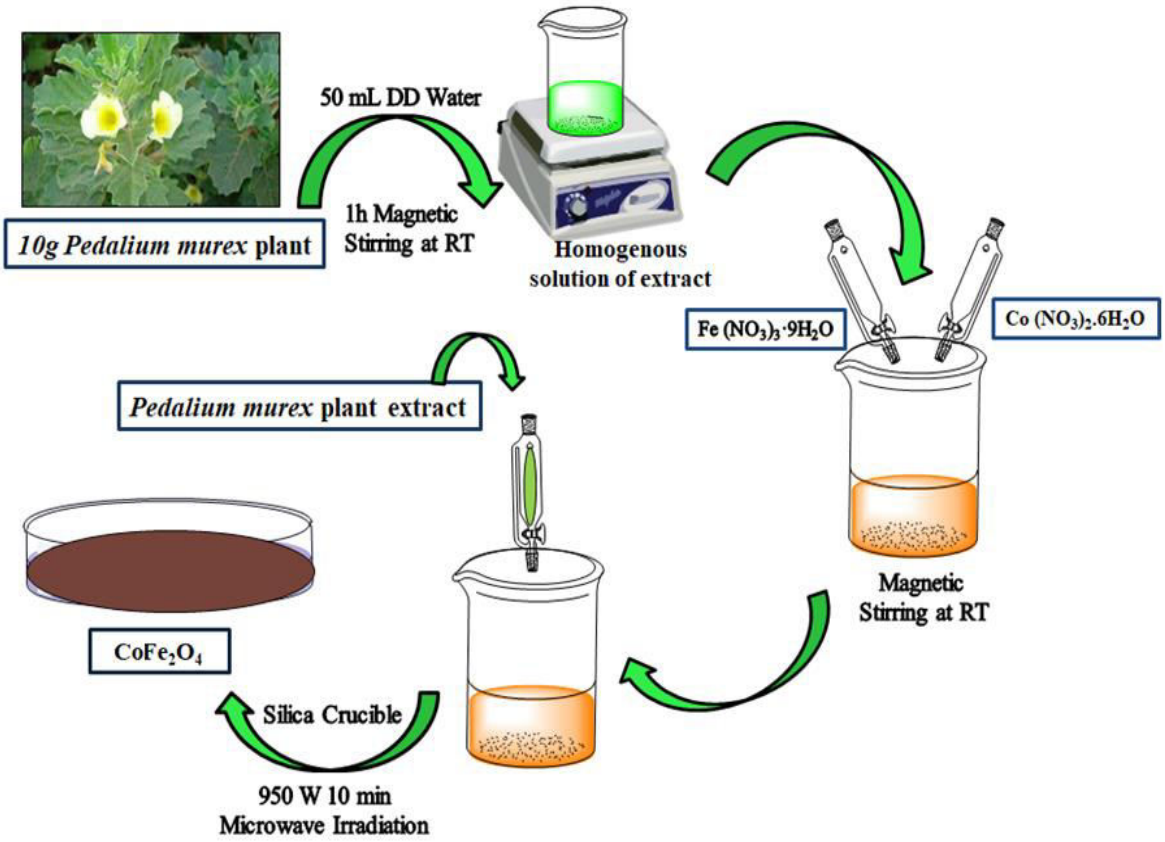

Scheme 1. Schematic diagram of preparation procedures of $CoFe_2O_4$ MNPs by a *Pedalium Murex* plant extract assisted microwave combustion method.

2.4 Synthesis of $CoFe_2O_4$ by conventional combustion method

The another part of the solution mixture was taken in the silica crucible and was placed in an air furnace and sintered at 500 °C at a heating rate of 5 °C/min for 2 h. Initially, the solution was boiled and dehydrated followed by decomposition with the evolution of gases. It vaporized the solution and slowly became a solid. After completion of the reaction, the obtained solid powder was then washed with ethanol and dried at 70 ºC for 1h. The obtained powders were labelled as $CoFe_2O_4$-CCM, prepared by CCM technique.

2.5. Characterization techniques

Structural characterization of nanocrystalline $CoFe_2O_4$ powders ($CoFe_2O_4$-MCM and $CoFe_2O_4$-CCM) was performed using a Rigaku Ultima IV high resolution powder X-ray diffractometer (XRD) with CuKα radiation at $\lambda = 1.5418$ Å. Structural refinements using the Rietveld method were carried out using PDXL program, both refined lattice parameters and crystallite size of the obtained ferrites were reported. The surface functional groups were analyzed by Perkin Elmer FT-IR spectrometer. Morphological studies and elemental chemical analysis have been performed with a Jeol JSM6360 high resolution scanning electron microscope (HR-SEM) equipped with energy dispersive X-ray (EDX) analysis. The transmission electron micrographs were carried out by Philips-TEM (CM20). The UV-visible

ISSN PRINT 2319 1775 Online 2320 7876

Research paper **© 2012 IJFANS. All Rights Reserved, UGC CARE Listed (Group -I) Journal Volume 11, Iss 8, Dec 2022**

diffuse reflectance spectrum (DRS) was recorded using Cary100 UV-Visible spectrophotometer to estimate their band gap energy. The photoluminescence (PL) properties were recorded using Varian Cary Eclipse Fluorescence Spectrophotometer. Magnetic measurements were carried out at room temperature using a PMC MicroMag 3900 model vibrating sample magnetometer (VSM) equipped with 1 Tesla magnet.

2.6. Antibacterial activity

The antibacterial activity (ABA) of spinel $CoFe_2O_4$-MCM and $CoFe_2O_4$-CCM samples was analysed by their zone of inhibitions on the human pathogens (HP) gram-positive *S. aureus (Staphylococcus aureus*), *B. subtilis* (*Bacillus subtilis*) *and* gram-negative *E. coli (Escherichia coli)* and *K. pneumonia (Klebsiella pneumoniae).* An instant culture of all microorganisms was attuned to an OD of 0.1 and wiped onto Mueller Hilton (MH) agar plates. By a cork borer (CB), holes were stamped on the agar, followed by adding of the standard solutions containing the synthesized $CoFe_2O_4$-MCM and $CoFe_2O_4$-CCM (10µg/mL). The plates were incubated at 37˚C for 24 h and the precinct of inhibitions on the human pathogens was dignified in diameter.

3. Results and discussions

3.1 Microwave combustion reaction

$CoFe_2O_4$-MCM MNPs were synthesized from an aqueous solution with metal nitrates, *Pedalium murex* plant extract and deionized water using via microwave combustion method. MCM route has more advantages as it does not need any more chemicals because of low budget, lack of by-product formation and an environmental friendly. In a microwave oven, microwave energy is absorbed by dealings of microwave radiation with the material and converted to thermal energy uniformly throughout a reaction container. MCM route has been rapidly developed as the energy of microwave reacts with the molecular level of reactants. Thus, by rapid heating of materials, faster kinetics, with better reproducibility of the products were observed

3.2. Powder XRD analysis

Figure 1 shows the XRD diagram of $CoFe_2O_4$-MCM and $CoFe_2O_4$-CCM MNPs. The XRD spectrum of the $CoFe_2O_4$-MCM shows three broad peaks at 2θ= 35.9, 57.2° and 62.3°. The XRD spectrum of $CoFe_2O_4$-CCM shows 5 sharp peaks at 2θ= 30°, 35.9°, 43°, 57.2°, and 62.8°. The peaks mentioned in two XRD spectra correspond to the cubic spinel structure of the $CoFe_2O_4$ [25, 26]. The crystallization degree of these $CoFe_2O_4$-MCM and $CoFe_2O_4$-CCM depends on the calcination time.

Sample Name	***L* (nm)**	**Lattice Parameter, *a* (Å)**	**Rietveld results**	
			Crystallite Size *L*(nm)	**Lattice constant**

ISSN PRINT 2319 1775 Online 2320 7876

Research paper © 2012 IJFANS. All Rights Reserved, UGC CARE Listed (Group -I) Journal Volume 11, Iss 8, Dec 2022

$CoFe_2O_4$-MCM	24.82	8.376	23.58	8.377
$CoFe_2O_4$-CCM	21.56	8.385	21.22	8.384

Table 1. Lattice parameter (a, Å), crystallite size (L) and bandgap (E_g, eV) energy of spinel $CoFe_2O_4$-MCM and $CoFe_2O_4$-CCM MNPs.

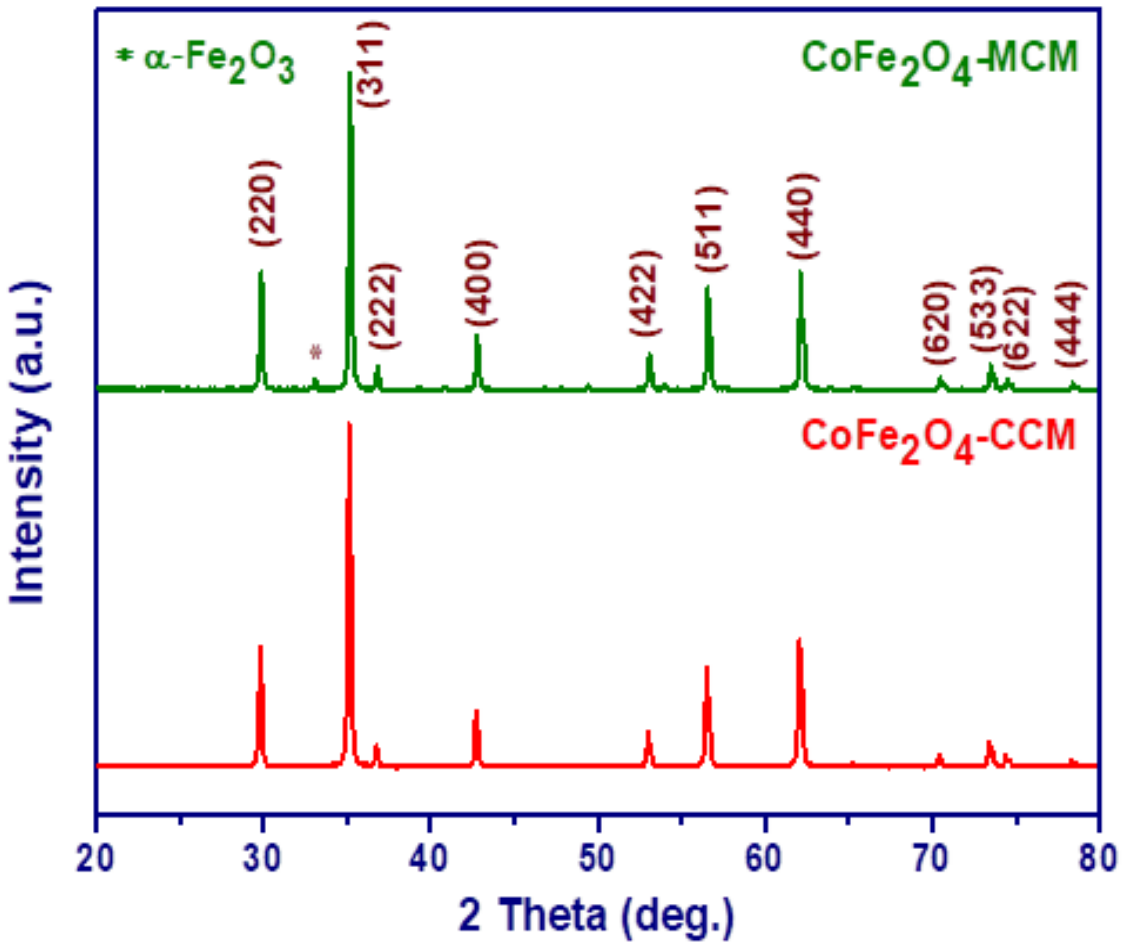

Fig. 1. Powder XRD pattern of spinel $CoFe_2O_4$-MCM and $CoFe_2O_4$-CCM MNPs.

In order to further analyse the structural change, the measured XRD patterns of the nanocrystals were simulated based on the Rietveld refinement method. Rietveld XRD data analysis for the nanocrystals is shown in Fig. 2. It was designed to refine simultaneously both the structural and microstructural parameters (i.e. Lattice constant and Crystallite size). During the refinements, the goodness of fit is defined by the reliability factor S = R_{wp}/R_e, where R_{wp} and R_e, are, respectively, the R_{wp}-weighted and the R_{ep}-expected patterns. The obtained values of the lattice parameter and crystallite size from the Rietveld analysis are shown in Table 1. The lattice parameter differs with methods from 8.376 to 8.385 Å.

ISSN PRINT 2319 1775 Online 2320 7876

Research paper **© 2012 IJFANS. All Rights Reserved, UGC CARE Listed (Group -I) Journal Volume 11, Iss 8, Dec 2022**

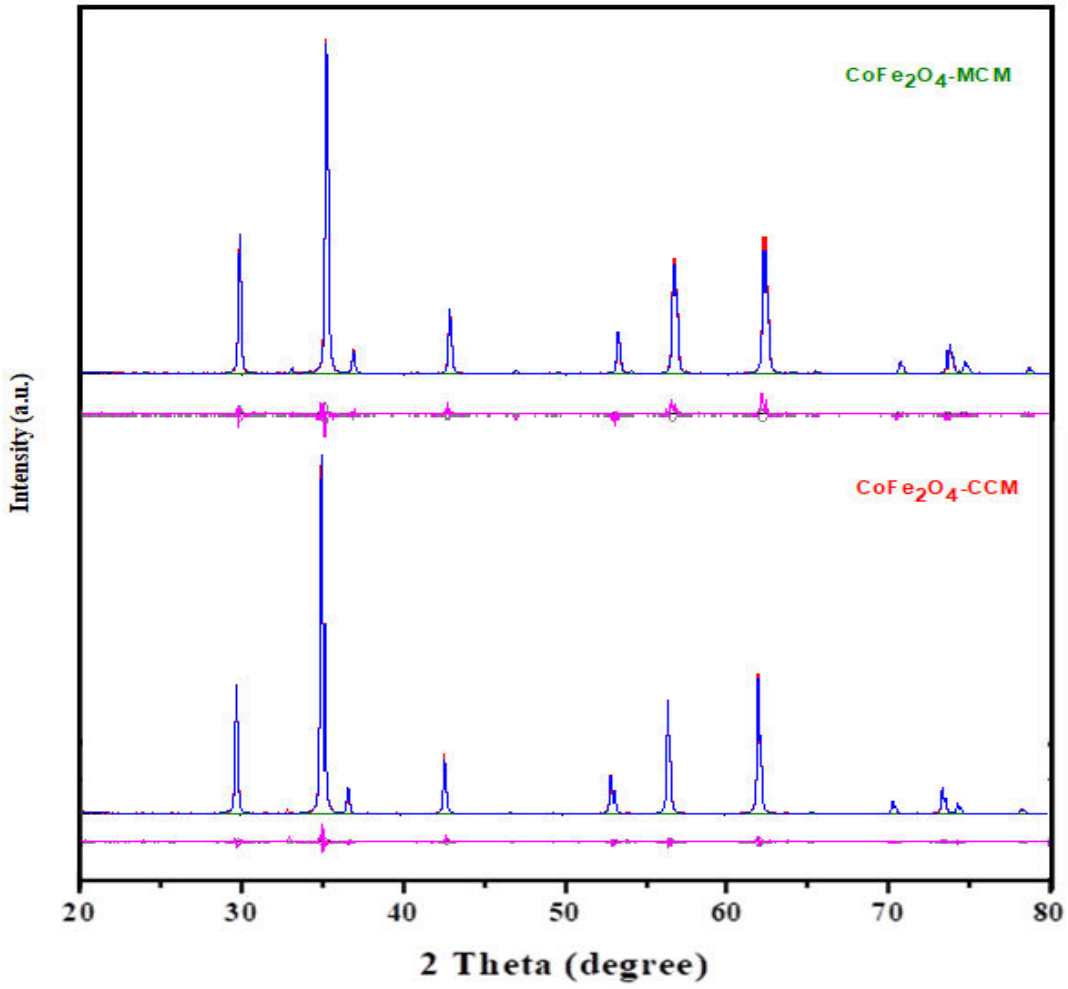

Fig. 2. Rietveld refinement XRD pattern of $CoFe_2O_4$-MCM and $CoFe_2O_4$-CCM MNPs.

3.3. HR-SEM analysis

Figure 3a,b show HR-SEM images of prepared $CoFe_2O_4$-MCM and $CoFe_2O_4$-CCM, respectively. The comparison of HR-SEM images and XRD spectra shows the difference in crystallization of $CoFe_2O_4$-MCM and $CoFe_2O_4$-CCM. HR-SEM images of the $CoFe_2O_4$-MCM and $CoFe_2O_4$-CCM confirmed the plate-like and spherical shaped surface morphology, respectively. Cubic and sheet-shaped plates with 19.56 nm wide illustrated that $CoFe_2O_4$-MCM did not crystallized well in a short time by MCM route (Figure 3a). As the crystallization time increases, the particles are formed in a regular and spherical manner of 25.48 nm (Figure 3b). Based on the results, by increasing the crystallization time, $CoFe_2O_4$-CCM were more spherical and smaller with higher particle size due to the temperature effect.

ISSN PRINT 2319 1775 Online 2320 7876

Research paper **© 2012 IJFANS. All Rights Reserved, UGC CARE Listed (Group -I) Journal Volume 11, Iss 8, Dec 2022**

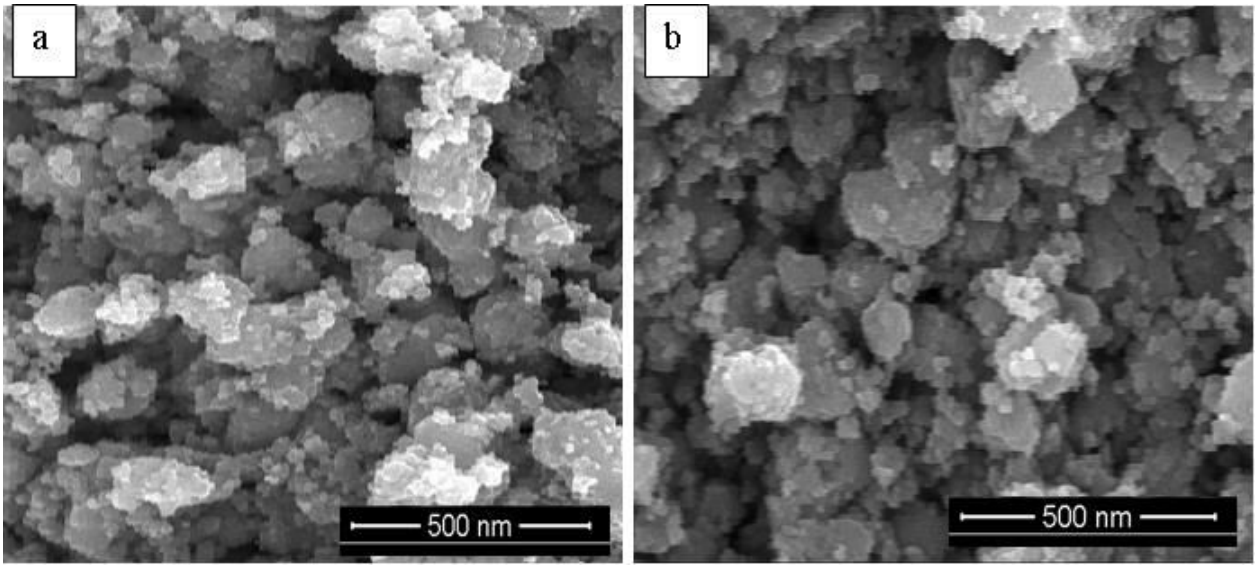

Fig. 3. HR-SEM images of (a) $CoFe_2O_4$-MCM and (b) $CoFe_2O_4$-CCM MNPs.

3.4. EDX analysis

Figure 4a,b show EDX spectra of as-prepared $CoFe_2O_4$-MCM and $CoFe_2O_4$-CCM, respectively. The presence of iron (56.5 w%), copper (15.5 w%), and oxygen (28.00 w%) confirmed the type of element constituents of $CoFe_2O_4$ [27-30]. A small peak was appeared at 2.1 KeV for both the samples, which indicated the presence of Au (gold) peak that has been used as a sputter coating, while preparing the sample for HR-SEM analysis for the better visibility of the surface morphology. The presence of the element carbon in the EDX diagram was due to the residues of the plant extract in the structure of $CoFe_2O_4$ (Figure 4a,b) [31].

ISSN PRINT 2319 1775 Online 2320 7876

Research paper **© 2012 IJFANS. All Rights Reserved, UGC CARE Listed (Group -I) Journal Volume 11, Iss 8, Dec 2022**

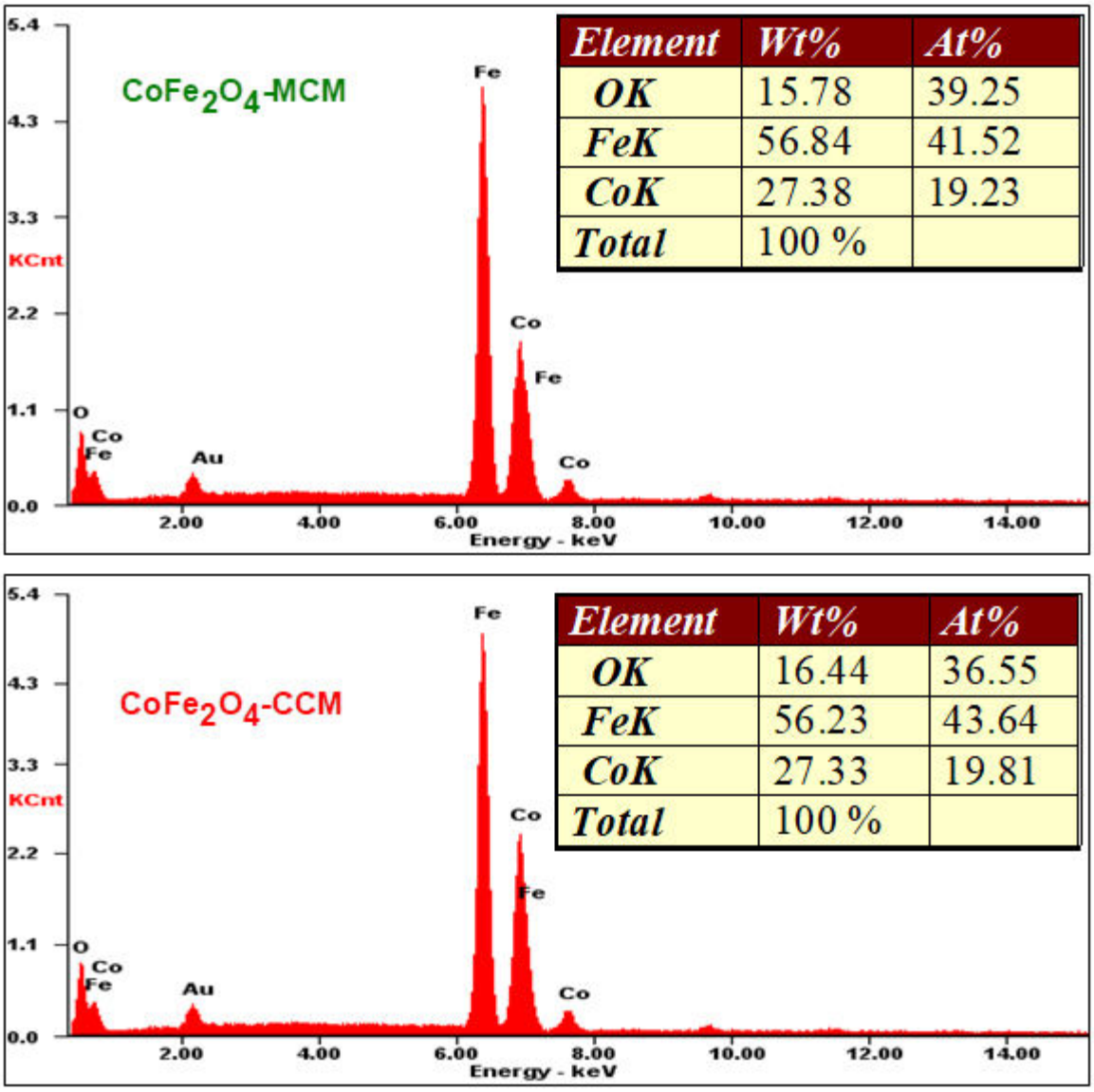

Fig. 4. EDX spectra of (a) $CoFe_2O_4$-MCM and (b) $CoFe_2O_4$-CCM MNPs.

3.5. HR-TEM analysis

Figure 5a,b show HR-TEM images of as-prepared $CoFe_2O_4$-MCM and $CoFe_2O_4$-CCM, respectively. It is clearly seen in Fig. 5a that $CoFe_2O_4$-MCM samples contain plate-like nanoparticles with particle sizes of ~ 19-17 nm, whereas $CoFe_2O_4$-CCM samples consist of many sphere-like nanoparticles (Fig. 5b) with particle sizes of ~ 23-48 nm, respectively. The average particle size that we can obtain from the HR-TEM images, is good agreement with the values obtained from powder XRD results [32-35].

ISSN PRINT 2319 1775 Online 2320 7876

Research paper **© 2012 IJFANS. All Rights Reserved, UGC CARE Listed (Group -I) Journal Volume 11, Iss 8, Dec 2022**

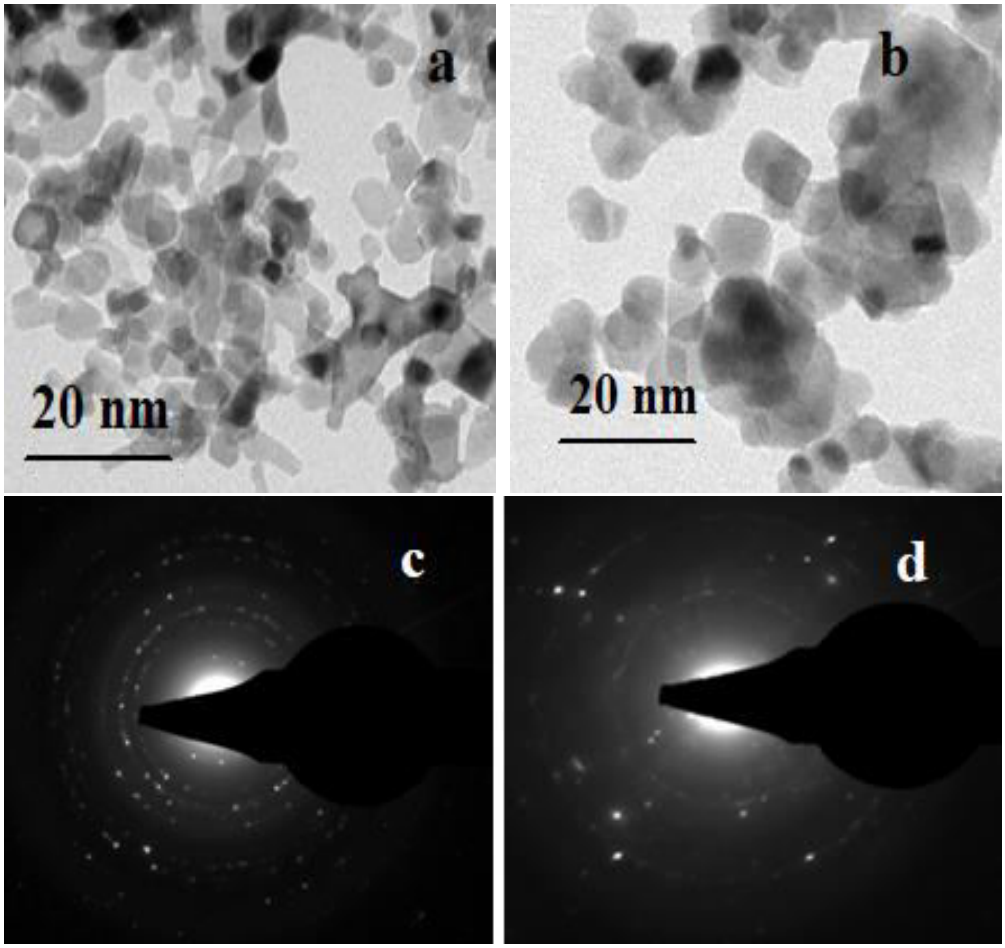

Fig. 5. HR-TEM images of (a) $CoFe_2O_4$-MCM and (b) $CoFe_2O_4$-CCM MNPs and SAED patterns of (c) $CoFe_2O_4$-MCM and (d) $CoFe_2O_4$-CCM MNPs.

Figure 5c, d show SAED images of as-prepared $CoFe_2O_4$-MCM and $CoFe_2O_4$-CCM, respectively show spotty ring patterns characteristic of well crystallites of the spinel ferrite without any additional diffraction spots/rings of secondary phases corresponding to the cobalt and iron oxides were observed. From the SAED pattern there are seven noticeable diffraction rings, the positions of which match well with standard powder diffraction information [36].

3.6. UV-Vis DRS spectral analysis

The optical properties of spinel $CoFe_2O_4$ nanostructures, UV-Vis. DRS studies were carried out at RT. The band gap energy (E_g) of the samples can be evaluated using Kubelka-Munk model. It allows the calculation of the absorption coefficient (α) by the measurement of the UV-Vis. diffuse reflectance and it is mainly used for powder samples. Kubelka-Munk function, F(R) is directly proportional to the absorption coefficient (α) and the value is estimated from the following equation,

ISSN PRINT 2319 1775 Online 2320 7876

Research paper **© 2012 IJFANS. All Rights Reserved, UGC CARE Listed (Group -I) Journal Volume 11, Iss 8, Dec 2022**

$$\left(F(R)\right) = \alpha = \frac{(1-R)^2}{2R} \qquad \text{------ (4)}$$

where, F(*R*) is Kubelka-Munk function, 'α', the absorbance, '*R*', the reflectance. A graph is plotted between $[F(R)h\upsilon]^2$ and $h\upsilon$, the intercept value is the band gap energy and are shown in Fig. 6a,b. The estimated band gap values of $CoFe_2O_4$-MCM and $CoFe_2O_4$-CCM are 2.06 eV and 1.88 eV, respectively. The higher band gap energy of $CoFe_2O_4$-MCM is indicating that the particle size approaches to nano regime than $CoFe_2O_4$-CCM. It is inferred that there is increase in the crystallite size in $CoFe_2O_4$-CCM, the band gap decreased. The significant feature is a direct relationship between grain size and optical band gap energy indicates a very weak quantum size effect [37-40].

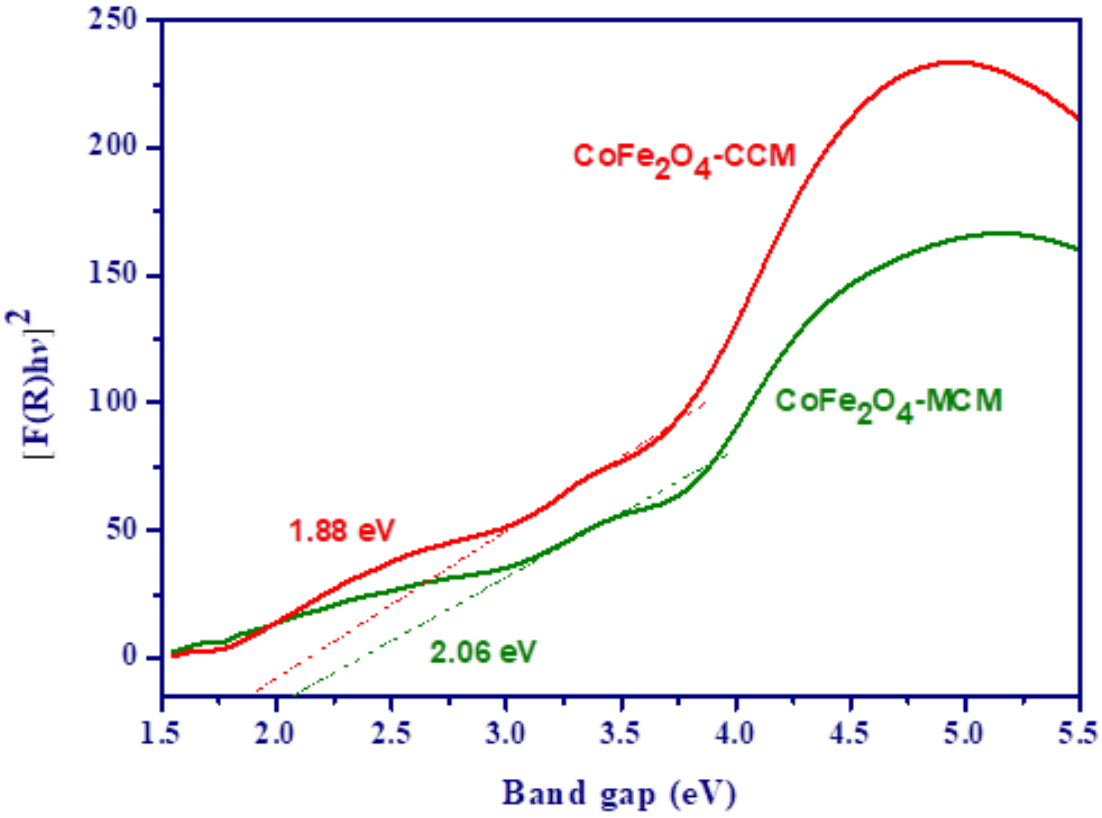

Fig. 6. Band gap values of $CoFe_2O_4$-MCM and $CoFe_2O_4$-CCM MNPs.

3.7. Photoluminescence (PL) spectroscopy

Photoluminescence (PL) spectroscopy was recorded at RT to investigate the recombination phenomena (RCP) of the oxide materials. Fig. 7a,b shows the RT- PL spectra of $CoFe_2O_4$-MCM and $CoFe_2O_4$-CCM, respectively recorded at the excitation wavelength of 235 nm. Two main PL peaks were observed at around 530 nm and 758 nm wavelength corresponding to 2.33 eV and 1.63 eV, respectively. The peaks at 422 nm and 453 nm correspond to the violet emission, due to the radiative defects related to the interface traps existing at the grain boundaries [41]. The main peak at 530 nm may be attributed to the oxygen vacancies giving rise to green emissions [42]. Yellow emissions are observed by the appearance of peak at 570 nm and 595 nm, which is attributed to the interstitial oxygen defects. In the deep level emission for all the samples display a defect-related visible luminescence band, which is

ISSN PRINT 2319 1775 Online 2320 7876

Research paper **© 2012 IJFANS. All Rights Reserved, UGC CARE Listed (Group -I) Journal Volume 11, Iss 8, Dec 2022**

usually related to the defects such as interstitial defect and oxygen vacancies [43]. The increase in the green emission (530 nm) intensity with decrease of crystallite size suggests the presence of various structural defects and the expansion of the band gap, E_g. The maximum emission is shifted to lower energies as the particle size is decreased, which might be related to the quantum confinement effect.

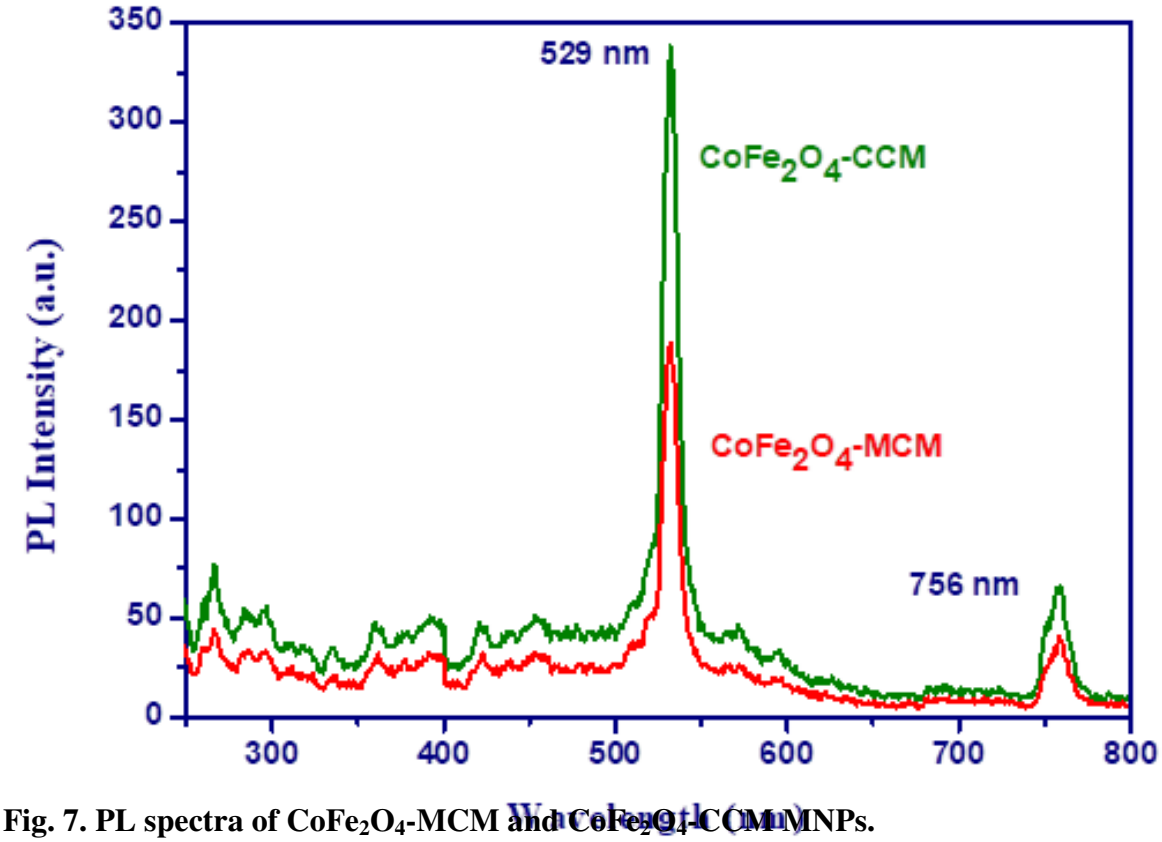

Fig. 7. PL spectra of $CoFe_2O_4$-MCM and $CoFe_2O_4$-CCM MNPs.

3.8. Fourier transform infrared (FT-IR) analysis

Fig. 8a,b shows the FT-IR spectra of $CoFe_2O_4$-MCM and $CoFe_2O_4$-CCM respectively. From the FT-IR spectra, it is found that two strong absorption peaks at lower frequency at around ~ 850 to ~ 430 cm^{-1} can be assigned to the stretching vibrations of the M-O bonds in A- and B-sites, respectively [44]. This can be attributed to the high degree of crystalline nature of $CoFe_2O_4$ nanostructures. A broad vibration band at ~ 3400 cm^{-1} is associated with the OH stretching vibrations indicating higher amount of surface hydroxyl groups, while those at ~ 1635 cm^{-1} are associated with their bending mode. Two weak bands at about 2934 cm^{-1} are assigned to C–H stretching vibrations. However, a weak band is observed at around ~ 2356 cm^{-1}, which indicating the CO_2 stretching frequency. Some weak but distinct bands in the range 1013 cm^{-1} are assigned to C–O bending modes. However, in this present investigation, we have observed two bands at around ~ 850 to ~ 430 cm^{-1} was confirmed the M-O bonds stretching vibrations in A- and B- sites of magnetic $CoFe_2O_4$ nanostructures [44]

ISSN PRINT 2319 1775 Online 2320 7876

Research paper **© 2012 IJFANS. All Rights Reserved, UGC CARE Listed (Group -I) Journal Volume 11, Iss 8, Dec 2022**

Fig. 8. FT-IR spectra of $CoFe_2O_4$-MCM and $CoFe_2O_4$-CCM MNPs.

3.9. VSM analysis

Figure 9a,b show VSM results of as-prepared $CoFe_2O_4$-MCM and $CoFe_2O_4$-CCM, respectively. The magnetic properties of the samples have been determined using RT-VSM in the applied filed range from -10 to +10 kOe. The magnetic hysteresis (M-H) loops for the nanocrystalline $CoFe_2O_4$ samples and the obtained magnetic parameters are shown Table 2. The amount of magnetic saturation (Ms) for the synthesized $CoFe_2O_4$-MCM and $CoFe_2O_4$-CCM was 82.55 and 67.28 emu/g, respectively. According to the literature, $CoFe_2O_4$ had superparamagnetic properties. Additionally, the amount of magnetic saturation of $CoFe_2O_4$ depends on their size [35].

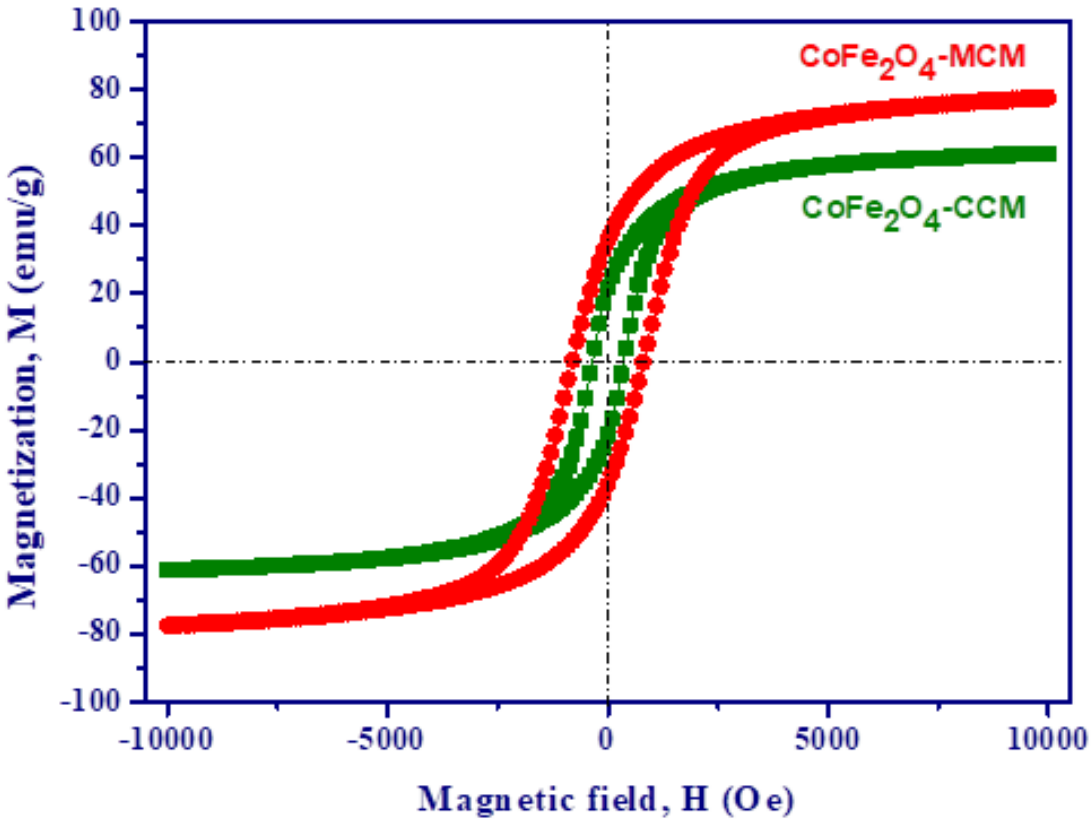

ISSN PRINT 2319 1775 Online 2320 7876

Research paper **© 2012 IJFANS. All Rights Reserved, UGC CARE Listed (Group -I) Journal Volume 11, Iss 8, Dec 2022**

Fig. 9. VSM measurements of $CoFe_2O_4$-MCM and $CoFe_2O_4$-CCM MNPs.

Table 2. Sample name, sample code, coercivity, remanant magnetization, saturation magnetization of $CoFe_2O_4$-MCM and $CoFe_2O_4$-CCM.

Samples Name	H_c, (O_e)	M_s (emu/g)	M_r (emu/g)
$CoFe_2O_4$-MCM	1035.86	82.55	42.56
$CoFe_2O_4$-CCM	884.62	67.28	28.55

3.10

Antibacterial activity

The antibacterial activity of spinel $CoFe_2O_4$-MCM and $CoFe_2O_4$-CCM magnetic nanoparticles (**Fig. 10**) were examined beside gram-positive *S. aureus (Staphylococcus aureus*), *B. subtilis* (*Bacillus subtilis) and* gram-negative *E. coli (Escherichia coli)*, *K. pneumonia (Klebsiella pneumoniae)* bacterial strains, correspondingly. From **Fig. 10**, it was originated that no zone of inhibition was obtained over the control. The obtained smaller particle size and higher surface area with the volume ratio of the $CoFe_2O_4$-MCM samples performance a vibrant character in the antibacterial activity of samples [35-38].

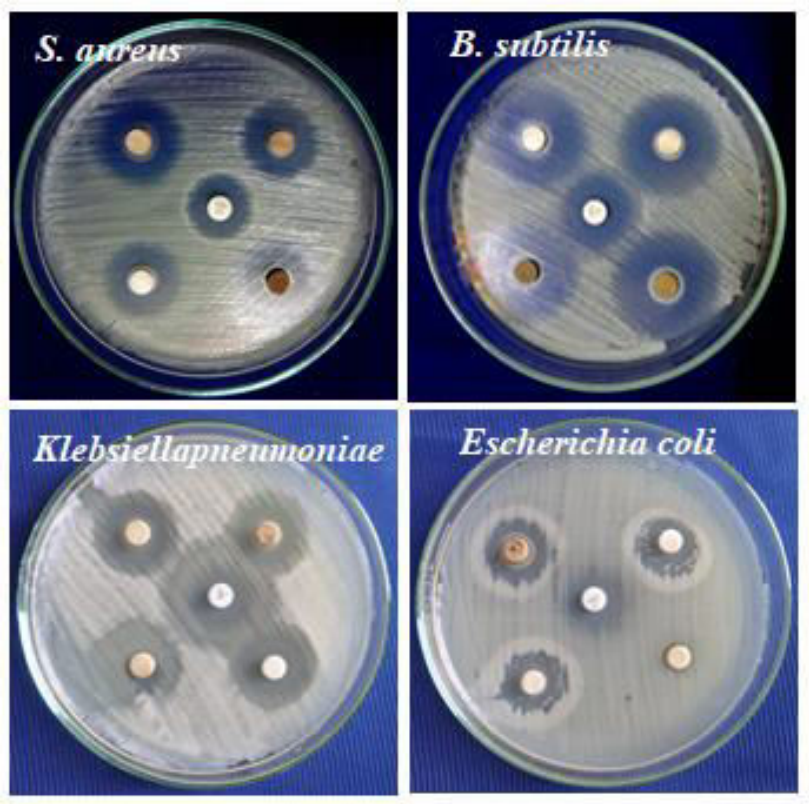

Figure 10. Antibacterial activity of $CoFe_2O_4$ nanoparticles against (a) *Staphylococcus aureus*, (b) *Bacillus subtilis*, (c) *Klebsiellapneumoniae* and (c) *Escherichia coli*

4. Conclusions

In this present study, $CoFe_2O_4$-MCM and $CoFe_2O_4$-CCM synthesised by a novel microwave and conventional combustion methods using metal nitrates and *Pedalium murex* plant extract.

ISSN PRINT 2319 1775 Online 2320 7876

Research paper **© 2012 IJFANS. All Rights Reserved, UGC CARE Listed (Group -I) Journal Volume 11, Iss 8, Dec 2022**

The powder XRD, EDX and SAED results indicate that the synthesized $CoFe_2O_4$ nanostructures have the spinel structure without the presence of any other phase impurities. The HR-SEM and HR-TEM results reveal that the $CoFe_2O_4$-MCM and $CoFe_2O_4$-CCM samples contain sphere-like and flake-like nanoplatelets, respectively. UV-Vis. DRS showed the band gap energy of $CoFe_2O_4$-MCM and $CoFe_2O_4$-CCM are 2.06 eV and 188 eV, respectively. The specific M_s values were obtained to be 82.55 and 67.28 emu/g at 10 kOe for the samples of $CoFe_2O_4$-MCM and $CoFe_2O_4$-CCM, respectively. The spinel structure and superparamagnetic behavior of these $CoFe_2O_4$ MNPs were confirmed by XRD and VSM analyses. Cobalt ions increased the surface to volume ratio in $CoFe_2O_4$, thus demonstrating good antibacterial properties against Gram-positive bacteria, *staphylococcus aureus*. In recent years, medicinal plants together with various nanomaterials can be considered as promising bio-medicines. Scientists are seeking to increase the medicinal plants effect of drugs by producing MNPs using plant extracts.

References

[1] Xi-Xi Wang, Wen-Qiang Cao, Mao-Sheng Cao, Jie Yuan, Assembling Nano–Microarchitecture for Electromagnetic Absorbers and Smart Devices, Adv. Mater. 32 (2020) 2002112.

[2] G. Padmapriya, A. Manikandan, V. Krishnasamy, S. K. Jaganathan, S. A. Antony, Spinel $Ni_xZn_{1-x}Fe_2O_4$ ($0.0 \leq x \leq 1.0$) nano-photocatalysts: Synthesis, characterization and photocatalytic degradation of methylene blue dye, J. Mol. Struct., 1119 (2016) 39-47.

[3] Mao-Sheng Cao, Xi-Xi Wang, Min Zhang, Jin-Cheng Shu, Wen-Qiang Cao, Hui-Jing Yang, Xiao-Yong Fang, Jie Yuan, Electromagnetic Response and Energy Conversion for Functions and Devices in Low-Dimensional Materials, Adv. Funct. Mater. 29 (2019) 1807398.

[4] S. Rehman, M. A. Almessiere, S. S. Al-Jameel, U. Ali, Y. Slimani, N. Taskhandi, N. S. Al-Saleh, A. Manikandan, F. A. Khan, E. A. Al-Suhaimi, A. Baykal, Designing of $Co_{0.5}Ni_{0.5}Ga_xFe_{2-x}O_4$ ($0.0 \leq x \leq 1.0$) Microspheres via Hydrothermal Approach and Their Selective Inhibition on the Growth of Cancerous and Fungal Cells, Pharmaceutics, 13 (2021) 962.

[5] Bo Wen, Maosheng Cao, Mingming Lu, Wenqiang Cao, Honglong Shi, Jia Liu, Xixi Wang, Haibo Jin, Xiaoyong Fang, Wenzhong Wang, Jie Yuan, Reduced Graphene Oxides: Light-weight and High-efficiency Electromagnetic Interference Shielding at Elevated Temperatures, Adv. Mater., 26 (2014) 3484–3489.

[6] M. Cao, X. Wang, W. Cao, X. Fang, B. Wen, and J. Yuan, Thermally driven transport and relaxation switching self-powered electromagnetic energy conversion, Small 14 (2018) 1800987.

[7] O. Alagha, N. Ouerfelli, H. Kochkar, M. A. Almessiere , Y. Slimani, A. Manikandan, A. Baykal, A. Mostafa, M. Zubair, M. H. Barghouthi, Kinetic Modeling for Photo-Assisted Penicillin G Degradation of $(Mn_{0.5}Zn_{0.5})[Cd_xFe_{2-x}]O_4$ ($x \leq 0.05$) Nanospinel Ferrites, Nanomaterials, 11 (2021) 970.

[8] Jin-Cheng Shu, Mao-Sheng Cao, Min Zhang, Xi-Xi Wang, Wen-Qiang Cao, Xiao-Yong Fang and Mao-Qing Cao, Molecular Patching Engineering to Drive Energy Conversion as Efficient and Environment-Friendly Cell toward Wireless Power Transmission, Adv. Funct. Mater., 2020, 30, 1908299.

[9] M. R. Ranjitha, A. Manikandan, J. N. Baby, K. Panneerselvam, S. Ragu, Mary George, Y. Slimani, M.A. Almessiere, A. Baykal, Hexagonal basalt-like ceramics $La_xMg_{1-x}TiO_3$ (x = 0

ISSN PRINT 2319 1775 Online 2320 7876

Research paper **© 2012 IJFANS. All Rights Reserved, UGC CARE Listed (Group -I) Journal Volume 11, Iss 8, Dec 2022**

and 0.5) contrived via deep eutectic solvent for selective electrochemical detection of dopamine, Physica B: , 615 (2021) 413068.
[10] Z. Chen, C. Xu, C. Ma, W. Ren and H. M. Cheng, Lightweight and Flexible Graphene Foam Composites for High-Performance Electromagnetic Interference Shielding, Adv. Mater., 25 (2013) 1296–1300.
[11] T. Liu, Y. Pang, M. Zhu, S. Kobayashi, Microporous Co@CoO nanoparticles with superior microwave absorption properties, Nanoscale, 6 (2014) 2447-2454.
[12] L. Liu, Y. Duan, L. Ma, S. Liu and Z. Yu, Microwave absorption properties of a wave-absorbing coating employing carbonyl-iron powder and carbon black, Appl. Surf. Sci., 257 (2010) 842–846.
[13] S. S. Al-Jameel, M. A. Almessiere, F. A. Khan, N. Taskhandi, Y. Slimani, N. S. Al-Saleh, A. Manikandan, E. A. Al-Suhaimi, A. Baykal, Synthesis, Characterization, Anti-Cancer Analysis of $Sr_{0.5}Ba_{0.5}Dy_xSm_xFe_{8-2x}O_{19}$ ($0.00 \leq x \leq 1.0$) Microsphere Nanocomposites, Nanomaterials, 11 (2021) 700.
[14] M. Mishra, A.P. Singh, B.P. Singh, V.N. Singh, S.K. Dhawan, Conducting ferrofluid: a high-performance microwave shielding material, J. Mater. Chem. A, 2:32 (2014) 13159-13168.
[15] M. A. Almessiere, Y. Slimani, H. Güngüneş, K. A. Demir, Z. Tatiana, T. Sergei, T. Alex, A. Manikandan, A. Fatimah, A. Baykal, Influence of Dy^{3+} ions on microstructure, magnetic, electrical and microwave properties of $[Ni_{0.4}Cu_{0.2}Zn_{0.4}](Fe_{2-x}Dy_x)O_4$ ($0.00<x<0.04$) spinel ferrites, ACS Omega, 6 (2021) 10266-10280.
[16] L. Wang, Y. Huang, X. Sun, H. Huang, P. Liu, M. Zong, Y. Wang, Synthesis and microwave absorption enhancement of graphene@Fe_3O_4@SiO_2@NiO nanosheet hierarchical structures, Nanoscale, 6:6 (2014) 3157-3164.
[17] M. A. Almessiere, Y. Slimani, İ. A. Auwal, S. E. Shirsath, A. Manikandan, A. Baykal, B. Özçelik, I. Ercan, Sergei V. Trukhanov, Denis A. Vinnik, A. V. Trukhanov, Impact of Tm^{3+} and Tb^{3+} Rare Earth Cations Substitution on the Structure and Magnetic Parameters of Co-Ni Nanospinel Ferrite, Nanomaterials, 10 (2020) 2384.
[18] Xiao-Juan Zhang, Guang-Sheng Wang, Wen-Qiang Cao, Yun-Zhao Wei, Jun-Fei Liang, Lin Guo, and Mao-Sheng Cao, Enhanced Microwave Absorption Property of Reduced Graphene Oxide (RGO)-$MnFe_2O_4$ Nanocomposites and Polyvinylidene Fluoride. *ACS Applied Materials & Interfaces* 2014, *6* (10) 7471-7478.
[19] N. A Algarou, Y. Slimani, M. A. Almessiere, A. Sadaqat, A. V. Trukhanov, M. A. Gondal, A. S. Hakeem, S. V. Trukhanov, M. G. Vakhitov, D. S. Klygach, A. Manikandan, A. Baykal, Functional $Sr_{0.5}Ba_{0.5}Sm_{0.02}Fe_{11.98}O_4$/x($Ni_{0.8}Zn_{0.2}Fe_2O_4$) Hard–Soft Ferrite Nanocomposites: Structure, Magnetic and Microwave Properties, Nanomaterials, 10 (2020) 2134.
[20] Q. Song, Z.J. Zhang, Controlled Synthesis and Magnetic Properties of Bimagnetic Spinel Ferrite $CoFe_2O_4$ and $MnFe_2O_4$ Nanocrystals with Core–Shell Architecture, J Am Chem Soc., 134 (2012) 10182-10190.
[21] S. Suguna, S. Shankar, S. K. Jaganathan, A. Manikandan, Novel synthesis of spinel $Mn_xCo_{1-x}Al_2O_4$ (x = 0.0 to 1.0) nano-catalysts: Effect of Mn^{2+} doping on structural, morphological and opto-magnetic properties, J. Supercond. Nov. Magn., 30 (2017) 691–699.
[22] P. Liu, Z. Yao, J. Zhou, Preparation of reduced graphene oxide/$Ni_{0.4}Zn_{0.4}Co_{0.2}Fe_2O_4$ nanocomposites and their excellent microwave absorption properties, Ceram Int., 41 (2015) 13409-13416.
[23] A. Silambarasu, A. Manikandan, K. Balakrishnan, Room temperature superparamagnetism and enhanced photocatalytic activity of magnetically reusable spinel $ZnFe_2O_4$ nano-catalysts, J. Supercond. Nov. Magn., 30 (2017) 2631–2640.

ISSN PRINT 2319 1775 Online 2320 7876

Research paper **© 2012 IJFANS. All Rights Reserved, UGC CARE Listed (Group -I) Journal Volume 11, Iss 8, Dec 2022**

[24] M. Fu, Q. Jiao, Y. Zhao, Preparation of $NiFe_2O_4$nanorod–graphene composites *via* an ionic liquid assisted one-step hydrothermal approach and their microwave absorbing properties, J. Mater. Chem. A, 1 (2013) 5577-5586.
[25] V. Sunny, P. Kurian, P. Mohanan, M.R. Anantharaman, A Flexible Microwave Absorber Based on Nickel Ferrite Nanocomposite, J. Alloy Compd, 489 (2010) 297-303.
[26] P. Liu, Z. Yao, J. Zhou, Controllable synthesis and enhanced microwave absorption properties of silane-modified $Ni_{0.4}Zn_{0.4}Co_{0.2}Fe_2O_4$ nanocomposites covered with reduced graphene oxide, RSC Adv., 5 (2015) 93739-93748.
[27] G. Mathubala, A. Manikandan, S. A. Antony, P. Ramar, Enhanced photocatalytic activity of spinel $Cu_xMn_{1-x}Fe_2O_4$ nanocatalysts for the degradation of methylene blue dye and opto-magnetic properties, Nanosci. Nanotech. Lett., 8 (2016) 375-381.
[28] K. Chen, C. Xiang, L. Li, H. Qian, Q. Xiao, F. Xu, A novel ternary composite: fabrication, performance and application of expanded graphite/polyaniline/$CoFe_2O_4$ ferrite, J. Mater. Chem., 22(2012) 6449-6455.
[29] Y. Slimani, M. A. Almessiere, A. D. Korkmaz, H. Güngüneş, M.Sertkol, A. Manikandan, A. Yildiz, S. Akhtar, Sagar E. Shirsath, $Ni_{0.4}Cu_{0.2}Zn_{0.4}Tb_xFe_{2-x}O_4$ nanospinel ferrites: Ultrasonic synthesis and physical properties, Ultrasonics Sonochemistry, 59 (2019) 104757.
[30] F. Wu, Y. Xia, Y. Wang and M. Wang, Two-step reduction of self-assembed three-dimensional (3D) reduced graphene oxide (RGO)/zinc oxide (ZnO) nanocomposites for electromagnetic absorption, J. Mater. Chem. A, 2 (2014) 20307–20315.
[31] C. Barathiraja, A. Manikandan, A. M. U. Mohideen, S. Jayasree, S. A. Antony, Magnetically recyclable spinel $Mn_xNi_{1-x}Fe_2O_4$ (x = 0.0–0.5) nano-photocatalysts: Structural, morphological and opto-magnetic properties, J. Supercond. Nov. Magn., 29 (2016) 477-486.
[32] Sasha Stankovich, Dmitriy A. Dikin, Richard D. Piner, Kevin A. Kohlhaas, Alfred Kleinhammes, Yuanyuan Jia , Yue Wu , SonBinh T. Nguyen, Rodney S. Ruof, Synthesis of graphene-based nanosheets via chemical reduction of exfoliated graphite oxide, Carbon, 45 (2007) 1558.
[33] Y.F. Zhu, Q.Q. Ni, Y.Q. Fu, One-dimensional barium titanate coated multi-walled carbon nanotube heterostructures: synthesis and electromagnetic absorption properties, RSC Adv., 5 (2015) 3748.
[34] A. M. Jacintha, A. Manikandan, K. Chinnaraj, S. A. Antony, P. Neeraja, Comparative studies of spinel $MnFe_2O_4$ nanostructures: Structural, morphological, optical, magnetic and catalytic properties, J. Nanosci. Nanotech., 15 (2015) 9732-9740.
[35] T.N. Lambert, T.N. Lambert, C.A. Chavez, B. H-Sanchez, P. Lu, N.S. Bell, A. Ambrosini, T. Friedman, T.J. Boyle, D.R. Wheeler, D.L. Huber, Synthesis and Characterization of Titania−Graphene Nanocomposites, J. Phys. Chem. C, 113 (2009) 19812.
[36] M. George, T.L. Ajeesha, A. Manikandan, A. Anantharaman, R.S. Jansi, E. R. Kumar, Y. Slimani, M.A. Almessiere, A. Baykal, Evaluation of Cu-$MgFe_2O_4$ spinel nanoparticles for photocatalytic and antimicrobial activates, J. Phys. Chem. Solids, 153 (2021) 110010.
[37] R.C. Che, L.M. Peng, X.F. Duan, Q. Chen, X.L. Liang, Microwave Absorption Enhancement and Complex Permittivity and Permeability of Fe Encapsulated within Carbon Nanotubes, Adv. Mater., 16 (2004)401-405.
[38] G. Mathubala, A. Manikandan, S. A. Antony, P. Ramar, Photocatalytic degradation of methylene blue dye and magneto-optical studies of magnetically recyclable spinel $Ni_xMn_{1-x}Fe_2O_4$ (x = 0.0-1.0) nanoparticles, J. Mol. Struct., 1113 (2016) 79-87.

ISSN PRINT 2319 1775 Online 2320 7876

Research paper **© 2012 IJFANS. All Rights Reserved, UGC CARE Listed (Group -I) Journal Volume 11, Iss 8, Dec 2022**

[39] B. Chandra Sekhar, G.S.N. Rao, O.F. Caltun, B. Dhana Lakshmi, B. Parvatheeswara Rao, P.S.V. Subba Rao, Magnetic and magnetostrictive properties of Cu substituted Co-ferrites. J. Magn. Magn. Mater. 339 (2016) 59-63.
[40] S.M. Ansari, S.R. Suryawanshi, M.A. More, D. Sen, Y.D. Kolekar, C.V. Ramana, Field emission properties of nano-structured cobalt ferrite ($CoFe_2O_4$) synthesized by low-temperature chemical method. Chemical Physics Letters 701 (2018) 151-156.
[41] M.P. Ghosh, S. Mukherjee, Microstructural, magnetic, and hyperfine characterizations of Cu-doped cobalt ferrite nanoparticles. J. Am. Chem. Soc. 102 (2019) 7509-7520.
[42] P. Saini, M. Arora, G. Gupta, K.B. Gupta, V.N. Singh, V. Choudhary, High permittivity polyaniline–barium titanate nanocomposites with excellent electromagnetic interference shielding response, Nanoscale, 5 (2013) 4330-4336.
[43] Yan-Jing Li, Shu-Long Li, Pei Gong, Ya-Lin Li, Xiao-Yong Fang, Ya-Hui Jia, Mao-Sheng Cao, Effect of surface dangling bonds on transport properties of phosphorous doped SiC nanowires. Physica E, 104 (2018) 247–253.
[44] Ya-Hui Jia, Pei Gong, Shu-LongLi, Wan-Duo Ma, Xiao-Yong Fang, Ying-Ying Yang, Mao-Sheng Cao, Effects of hydroxyl groups and hydrogen passivation on the structure, electrical and optical properties of silicon carbide nanowires, Physics Letters A, 384 (2020) 126106.